



# Unprecedented quiescence in resource development area allows detection of long-lived latent seismicity

Rebecca O. Salvage<sup>1</sup> and David W. Eaton<sup>1</sup>

<sup>1</sup>Dept. of Geoscience, University of Calgary, Calgary, AB, T2N 1N4

**Correspondence:** Rebecca O. Salvage (beckysalvage@gmail.com)

**Abstract.** Recent seismicity in Alberta and British Columbia has been attributed to ongoing oil and gas development in the area, due to its temporal and spatial correlation. Prior to such development, the area was seismically quiescent. Here, we show evidence that latent seismicity may occur in areas where previous operations may have occurred, even during a shutdown in operations. The global pandemic of COVID-19 furnished the unique opportunity to study seismicity during a period of anthropogenic quiescence. A total of 389 events were detected within the Kiskatinaw area of British Columbia from April to August 2020, which encompasses a period with no hydraulic fracturing operations during a government imposed lockdown. Apart from a reduction in seismicity rate, the general characteristics of the observed seismicity were similar to the preceding time period of active operations. During the shutdown, observed event magnitudes fell between  $M_L -1$  and  $M_L 1.2$ , but lacked temporal clustering that is often characteristic of hydraulic-fracturing induced sequences. Hypocenters occurred in a corridor orientated NW-SE, just as seismicity had done in previous years in the area, and locate at depths associated with the target Montney formation or shallower ( $<2.5$  km). A maximum of 21% of the detected events during lockdown may be attributable to natural seismicity, with a further 8% being attributed to dynamic triggering of seismicity from teleseismic events. However this leaves over 70% of the seismicity detected during lockdown being unattributable to primary activation mechanisms. Since we know this seismicity cannot be the result of direct pore-pressure increases (as no direct injection was occurring at the time) and we see no patterns of temporal or spatial migration in the seismicity, we suggest that this latent seismicity may be generated by aseismic slip as fluids (resulting from previous hydraulic fracturing experiments) become trapped within permeable formations at depth, keeping pore pressures in the area elevated, and consequently allowing the generation of seismicity. This is the first time that this latent seismicity has been observed in this area of British Columbia.

## 1 Introduction

The number of recorded instances of injection-induced seismicity has risen dramatically over the past decade, in part due to increased operations in hydraulic fracturing, waste-water disposal and enhanced geothermal systems around the globe, as well as enhanced monitoring meaning we are better able to detect smaller events (e.g. Atkinson et al., 2016; Ellsworth, 2013). In western Canada, the Western Canadian Sedimentary Basin (WCSB) is the focus on such activity, where a number of distinct resource plays are located including the Montney and the Duvernay. Despite an apparent flurry of larger magnitude seismic events associated with these operations (e.g.  $M_L 4.5$  near Fort St John, British Columbia in November 2018, Babaie-Mahani



et al. (2019); Peña Castro et al. (2020);  $M_W$  4.1 near Fox Creek, Alberta in January 2016, Eyre et al. (2019b)) very few hydraulic fracturing operations ( $\sim 0.3\%$ ) are actually linked to seismic activity with  $M_W > 3$  (Atkinson et al., 2016).

30 The Montney Play which is Lower-Middle Triassic in age, is formed of extensive fine-grained siliclastic units (inter-bedded sand, silt and mudstones), and stretches from west-central Alberta to north-east British Columbia (Eaton and Schultz, 2018; Dixon, 2000; Armitage, 1962). Over 5,600 multistage horizontal hydraulically fractured wells had been completed within the Montney by December 2018 (Nieto et al., 2018). In recent years, north-east British Columbia has experienced an increasing number of felt seismic events during active development within the Montney play. This led the BC Oil and Gas Commission to implement a special order in 2018, within the area now known as the Kiskatinaw Seismic Monitoring and Mitigation Area  
35 (KSMMA), which required operators to undertake a pre-assessment of the seismic hazard, fully inform residents in the area of upcoming operations and real-time seismic monitoring before, during and after completions (BC Oil and Gas Commission, 2018). Of particular importance was the introduction of the threshold for the cessation of operations following a  $M_L$  3.0 or above within the KSMMA, which is lower than the  $M_L$  4.0 threshold that is standard elsewhere in British Columbia (e.g. Babaie-Mahani and Kao, 2020).

40

Prior to the introduction of oil and gas extraction, western Canada was generally seismically quiet, except for the Mackenzie Mountains and the North American plate boundary off the west coast of British Columbia (Lamontagne et al., 2008). Consequently seismicity detected within the KSMMA has been assumed to be directly related to ongoing operations due to its temporal and spatial correlation with active wells. However, there are a number of examples of seismicity thought to be related to hydraulic  
45 fracturing that generate events months after operations have ceased (e.g. Eyre et al., 2020). We call this latent seismicity i.e. seismicity that appears after an unusually long delay following primary activation processes with no obvious “trigger” (e.g. enhanced pressurization at the onset of seismicity), and which cannot be explained by other sources (e.g. natural or dynamic triggering processes).

50 Here, we investigate seismicity generated within the KSMMA during the unprecedented period of quiescence that resulted due to the global COVID-19 pandemic. The cessation of operations in the area and the reduction in seismic noise as businesses shut down and people stayed indoors gave us the unique opportunity to study latent seismicity in an area where it would usually go undetected. Given that prior to the development of the Montney play this area was characteristically quiet in terms of natural seismicity (Lamontagne et al., 2008), the detection of latent seismicity over  $\sim 4$  months suggests lingering changes in the stress  
55 field to allow for its generation.

## 2 COVID-19 and the reduction of noise globally

The year 2020 was unusual due to the global pandemic that caused the shutdown of many businesses and severely restricted the movement of people worldwide. This reduction in ground motion has been accurately measured by a drop in seismic ambient



noise in many places, and correlated with a decrease in population mobility (e.g. Lecocq et al., 2020; Dias et al., 2020).

60

The noise level at a seismic station can be estimated using the probabilistic power spectral density (PPSD) of its records (McNamara and Buland, 2004). Following the methodology of Lecocq et al. (2020) we compute the PPSD from 30-minute windows with 50 percent overlap so that a single value is gained for each window, calculated using Welch's method (Welch, 1967) for the Z-component of different seismic stations. This method reduces numerical noise in the power spectra at the expense of reducing the frequency resolution because of frequency binning, but this effect is minimized with a robust smoothing parametrization. The 30-minute time series are then converted to an average daily PSD, and the RMS of the time-domain displacement is extracted. Anthropogenic cultural noise typically concentrates at high frequencies ( $> 1$ -10 Hz, McNamara and Buland (2004)), but is strongly diurnal (e.g. stronger during the day than at night, and stronger during the weekdays compared to the weekends (Lecocq et al., 2020)). To avoid meteorological signals, and in particular oceanic microseisms (which typically manifest below 1 Hz), we use the frequency band of 4-14 Hz to investigate seismic noise during the pandemic.

70

Figure 1 shows the reduction of seismic noise in the frequency band 4-14 Hz in Gastown, Vancouver, BC during the global pandemic. A clear reduction in noise is observed following the closure of schools (black line) and businesses (red line). During Phase I of the pandemic (i.e. between the closure of businesses and the partial reopening of the city on 5 May 2020 (green line)), noise levels remain lower than previously recorded. Following the reopening of some businesses in May and June 2020, an increase in the noise is seen, although it remains lower than pre-pandemic levels, interpreted as the increased movement of people. To verify that these variations do not occur on an annual basis, we undertook the same noise analysis for the year 2019, and found no such fluctuations during the corresponding months. In fact, ground displacement remained between 20 and 30 nm at station R25AC for the entirety of 2019.

75

### 80 3 Seismicity in the KSMMA

With increasing oil and gas operations within the KSMMA over the past decade, the number of public monitoring stations has also increased. Prior to 2020, 9 public sensors maintained by Natural Resources Canada and the Geological Survey of Canada existed within the KSMMA boundary, along with 6 co-located accelerometers poised to better capture higher levels of ground motion from larger seismic events. In early 2020, 13 additional broadband seismic stations (Trillium T120 seismometers with Taurus digitizers) and two Titan accelerometers were installed within the KSMMA (expanding the EON-ROSE (EO) network) as part of a joint project between the University of Calgary, Nanometrics, Geoscience BC and a number of universities in South Korea to monitor ongoing seismicity associated with hydraulic fracturing operations (Salvage et al., 2021).

85

The catalogue of seismic events detected in the KSMMA is based on the newly installed array and available public stations in the area. Events were detected from the incoming continuous seismic data using an STA/LTA triggering algorithm, followed by a separate template-matching algorithm utilising continuously re-trained modules that classify noise from events and remove

90



unwanted signals. Then, a support vector machine (SVM) machine learning technique was used to identify phase arrivals in continuous real-time waveform streams. These phase arrivals are identified by training an SVM model on historical data. By converting the waveforms into over 250 features using quantities such as time and band-normalized spectrograms, a model is  
95 generated which can associate the features with P and S phases (or conversely, with noise).

We take the catalogue of event times and P and S phases, and determine hypocentre locations using NonLinLoc (Lomax et al., 2009, 2000), a probabilistic, global-search non-linear algorithm that generates the maximum likelihood hypocenter location based on the estimated posterior probability density function for each event. A 1D velocity model, specifically calibrated  
100 for the KSMMA from compressional and shear sonic logs, formation tops and ground truth locations of previous seismicity (available directly from BCOGC). Events were then re-located using HypoDD, a double difference algorithm, whereby the residual between the observed and calculated travel-time difference (or double-difference) between two earthquakes observed on a single station are related to differences in their relative hypocenter locations and origin times (Waldhauser and Ellsworth, 2000). To calculate magnitudes we use a form of the Richter (1935) magnitude formula that has been modified to better reflect  
105 local attenuation characteristics within the KSMMA (Babaie-Mahani and Kao, 2020). In line with calculations conducted by Natural Resources Canada (NRCan), we calculated  $M_L$  using the maximum amplitude from the vertical component simulated on a Wood-Anderson (WA) seismometer, rather than the horizontal component, which has been used elsewhere.

Historically, seismicity within the KSMMA appears to occur within spatially distinct regions that fall within a corridor  
110 orientated NW-SE (Fig. 2). In both years, the largest magnitude event occurred in an area away from the densest occurrence of seismicity. Since the largest event in 2020 did not occur in the same cluster as the largest event of 2018, it appears that the occurrence of  $M_L$  3-4+ events is not necessarily confined to a single region. Temporally, seismicity within the KSMMA occurs in distinct clusters, attributed to ongoing development activity in the area (Fig. 3). In 2018, heightened periods of seismicity were observed in April, May, July and August (Fig. 3(a)). Similar periods of heightened seismicity were observed  
115 in 2020 in March, August and September (Fig. 3(b)). The majority of seismicity detected within the KSMMA is  $M_L \leq 2$ , and consequently goes unfelt.

### 3.1 Prior and Post Lockdown: 2020

In March 2020, the Province of British Columbia introduced measures aimed at slowing the spread of COVID-19, including the closure of schools and childcare facilities on 17 March, and the closure of many businesses (in particular those that included  
120 daily human interaction) on 21 March. Up until this point in 2020, similar patterns of seismicity to other years were observed in the KSMMA (Fig. 3). A total of 4,268 events were detected from the onset of data collection (22 January 2020) from the updated EO array (yellow triangles, Fig. 2) to 1 April. Following the initial closure of businesses on 21 March, there is evidence of ongoing hydraulic fracture operations for  $\sim 10$  days, with associated heightened seismicity (Fig. 3(b)). It is possible this reflects operators in the area undertaking additional hydraulic fracturing jobs during this time, as government restrictions  
125 became increasingly tight, and no “end-date” to the restrictions being suggested, or it may be that these 10 days of seismicity



represent the continuation of planned operations with no initiation of new jobs. Magnitudes of recorded seismicity prior to lockdown at the end of March range from  $M_L$ -0.73 to  $M_L$ 2.93.

At the beginning of April, a period of relative seismic quiescence began in the KSMMA (Fig. 3(b)). Operations were once again restarted in British Columbia in the later summer months, after  $\sim$ 4 months. Seismicity since the resumption of activities is once again temporally clustered, with a total of 2,617 events being recorded since 6 August to present. The largest magnitude event of 2020 at the time of writing occurred on 11 September at 22:37 UTC with an estimated  $M_L$  of 3.1, after which proximal operations were shut down in line with the traffic light protocol introduced for the KSMMA (BC Oil and Gas Commission, 2018). A total of 73 precursory events occurred over approximately 4 hours, with events locating within a small spatial extent ( $\sim$ 300m x 150m), probably directly related to ongoing operations in the area due to the correlation in space and time of events and injection. Events within this precursory sequence had magnitudes between  $M_L$  0.2 and  $M_L$  2.6, and were all located at depths of approximately 2.05 km. Moment tensor results for this event suggest a focal mechanism dominated by strike-slip (Salvage et al., 2021).

### 3.2 Evidence of reduction in seismic noise

A clear reduction in the number of seismic events was observed during the lockdown period from April to August 2020 in the KSMMA (Fig. 3(b)). Over the  $\sim$  4 months of relative quiescence only 389 events were detected using the EO network and available public stations in the area. For comparison, 344 events were detected on our network over a single week from 8 to 15 February when operations were fully underway. On average during this period, the magnitude of events were smaller than during time periods when activity was driven by ongoing operations.

A reduction in seismic noise and therefore ground motion is also evident in the KSMMA following the introduction of government restrictions in March 2020 (Fig. 4). Unfortunately, the most central seismic stations in the EO array were not installed until immediately before (March) or post lockdown (May) and therefore could not be used to analyze the long term changes in seismic noise. We chose station KSM08, located in the east of KSMMA due to the long, uninterrupted seismic data recorded at this station, as well as its proximity to recent dense clusters of ongoing seismicity (Fig. 2). Heightened seismic ground motion is evident at KSM08 through January to March, as operations are ongoing (Fig. 4). A significant decrease in seismic ground motion is observed following the government restriction in late March 2020, with the average displacement sitting well below the weekday and weekend daytime mean calculated prior to lockdown. As restrictions ease, we see a large increase in ground motion following the reopening of businesses in May 2020, although this once again tails off through June and July. The re-introduction of operations in August is clear from an increase in ground displacement and seismic noise, which has remained elevated (although not as high a pre-lockdown levels) since.



### 3.3 Latent Seismicity during relative quiescence: 2020

Seismicity occurring during the period of quiescence from April to August 2020 within the KSMMA exhibit a number of characteristics indicative that it is a (latent) consequence of previous operations in the area. Figure 5 shows the temporal and spatial evolution of seismicity during this period. Firstly, perhaps unsurprisingly, seismicity does not occur in a distinct temporal pattern that exhibits clustering (Fig. 5(a)). A small number of events ( $\sim 5$ ) occur each day throughout the 4 months. Event magnitudes also reveal no discerning patterns with time, with all events registering  $M_L$ -0.66 to  $\sim M_L$  1.2. Furthermore, the frequency index (FI) suggests no temporal patterns during the period of relative quiescence. The FI is a proxy for the spectral content of each waveform based upon the ratio of energy in low and high frequency windows (Buurman and West, 2010), calculated at a single station. We use station KSM06 (Fig. 2) due to its proximity to the majority of the ongoing seismicity during this period of relative quiescence. A negative FI means the waveform is dominated by low frequency energy (in this case 1 - 40 Hz); a positive FI demonstrates a majority of energy in the high frequency band (40.1 - 80 Hz). In many environments (e.g. volcanic) a lower frequency content of the waveform is proposed as evidence for the direct role of fluids in the generation of the seismicity (e.g. Lahr et al., 1994; Chouet, 1996). The seismicity detected during the period of relative quiescence within the KSMMA shows no discerning temporal characteristics.

Spatially, seismicity detected during the COVID lockdown period exhibits characteristics that are similar to the previously detected seismicity in the KSMMA (Fig. 5(b)). Most events occur in a corridor orientated NW-SE, similar to the spatial distribution of seismicity prior to lockdown. Some spatial clustering is evident (e.g. in May in the south (yellow)), but given the limited number of events this is difficult to determine with certainty. Most events during the quiescence period occur at a focal depths of  $\sim 0$ -4 km, which is similar for events prior to lockdown within the KSMMA, if potentially slightly shallower. Target formations for hydraulic fracturing within the KSMMA (Upper and Lower Montney) typically sit between 2000 m and 2500 m (total vertical depth), with salt water disposal (SWD) injecting at shallower depths (M. Gaucher, Pers. Comm, 2020). This suggests that events detected during the quiescence were generated in formations similar to those that occur when active hydraulic fracturing and SWD is ongoing.

## 4 Discussion

### 4.1 Characteristics of Observed Seismicity

Seismicity generated during this period of quiescence appears to share many characteristics with seismicity generated during hydraulic fracturing operations within the KSMMA. Although low in number, the event rate per day remains fairly constant throughout the  $\sim 4$  month period of no hydraulic fracturing operations, with no apparent temporal decay (Fig. 5(a)). This contrasts the “usual” pattern of seismicity during active hydraulic fracturing operations, which is highly temporally (and spatially) clustered around the wells operating (Fig. 3) (e.g. Skoumal et al., 2015). Figure 3(b) also suggests no change in



the recorded magnitudes of events pre- and during lockdown.

190

The magnitude of completeness ( $M_c$ ) during the lockdown period is  $\sim 0.4$ . The  $M_c$  for the entire catalogue to from 22 January to 1 October 2020 ( $n=7216$ ) is estimated to be 0.074, suggesting that even though relatively few events were detected during this quiescence, the detection of small magnitude events is good. Given the reduction in noise during the period of quiescence (Fig. 4), this is perhaps no surprise. The estimated  $b$ -value (Gutenberg and Richter, 1944) of 1.96 is similar to  $b$ -values estimated from seismicity associated with hydraulic fracturing experiments in Western Canada, suggesting an abundance of lower magnitude events (Igonin et al., 2018; Eaton et al., 2014). The fact that no large magnitude events were detected during the period of quiescence (no  $M_L > 1.5$ ) is directly influencing the estimated  $b$ -value in this case. Interestingly, higher  $b$ -values have typically been attributed to seismicity generated in normal faulting regimes (Schorlemmer et al., 2005; Amini and Eberhardt, 2019). The KSMMA is strongly influenced by the Fort St. John Graben complex, an asymmetrical half graben that has also undergone significant strike-slip and rotational movement upon reactivation of the basement faults in the area (Barclay et al., 1990), which may also be directly influencing the estimated  $b$ -value. Furthermore, in hydraulic fracturing environments,  $b$ -values of  $> 2$  have been associated with the stimulation of natural fractures at depth, with smaller  $b$ -values associating with large-scale tectonic faults (Wessels et al., 2011; Eaton and Maghsoudi, 2015). In our case, this would suggest that the seismicity being generated is directly related to the complex natural fracture system, rather than any large scale faults in the area.

205

Seismicity during the quiescence appears to be spatially concurrent with previous seismicity in the area (Figs. 5(b) and 2). However, there appears to be very little correlation between the spatial extent of seismicity and the most recent hydraulic fracturing activity in the area (active in March 2020 prior to lockdown). Seismicity appears in two planar elongated features, extending in a NW-SE direction, with lengths of up to 30 km (eastern segment), if assumed to be one feature. These features are not coincident with any known faults in the area (Furlong et al., 2020). Seismicity recorded during this period of quiescence is generally located at a similar depth to the target formations of the Montney ( $\sim 2$  km), as well as in the formations above. This suggests hydraulically connected pathways above the injection zone, perhaps within mechanically stronger lithologies, as has been previously suggested by Eyre et al. (2019b) in the Fox Creek region of Alberta (another area undergoing intensive hydraulic fracturing operations).

215

The generation of induced seismicity has often been successfully correlated to a number of injection parameters, including the injected volume of fluid (e.g. Yu et al., 2019; Ellsworth, 2013) and/or the pumping rate (e.g. Goebel et al., 2017). Temporally data is too sparse to draw conclusions as to whether any of these parameters directly influence the generation of induced seismicity within the KSMMA, although given that hydraulic fracturing operations during our period of interest were ceased, we know that this seismicity cannot be a direct response of this type of fluid injection. However, there is evidence that a small number of seismic events identified from April to August 2020 may be associated with salt-water disposal (SWD). Within the KSMMA, only 8 SWD wells were active in 2020, compared to hundreds of hydraulic fracturing wells. Of these, only one well was active during our period of investigation (Fig 5b). We believe the seismicity occurring on 13 April 2020 (Fig. 5a, upper

220



panel), where over 20 events were registered on the same day (significantly above the background rate of seismicity during  
225 this quiescence), may be due to SWD. In this case, ongoing sustained SWD occurred  $\sim 2$  km away from the events occurring  
on this day. This offset is not unusual for SWD and associated seismicity; Schultz et al. (2014) found an offset of  $\sim 3.5$  km  
between SWD and associated seismicity in Alberta.

## 4.2 Estimation of Noise

PPSD is one of the most common methods used to characterize ambient seismic noise. However, the level of smoothing, the  
230 size of the data window used in analysis and the methodology itself may all influence the PPSD calculation and distort features  
of interest (Anthony et al., 2020). Smoothing is primarily undertaken in order to reduce the uncertainty associated with the  
PPSD estimates, and means that short spikes in noise (e.g. due to wind gusts or seismic activity) do not dominate the spectrum.  
In our case, the reduction in ground motion is much easier to determine from the average of the PPSD rather than individual  
estimates (Figs. 1 and 4, green vs. grey lines). Although we use a period smoothing of 0.025 octaves, this is likely to provide  
235 adequate spectral resolution of spectral peaks, as shown by Anthony et al. (2020) and therefore impacts our results minimally.  
We also use a window of 30 minutes (overlapping by 50%) to try to reduce spectral leakage and variance when calculating the  
PPSD.

Earthquakes, and other transient signals, are likely to impact the estimation of ambient noise by generating large spikes in  
240 the data. However, the removal of seismicity from datasets is generally accepted as not necessary since they are low-probability  
occurrences within generally high-probability ambient seismic noise (McNamara and Buland, 2004). Only teleseismic earthquakes  
appear to have any real affect upon PPSD calculations (Anthony et al., 2020). A number of teleseismic events have been  
detected in the KSMMA during the period of quiescence analysis (e.g.  $M_w$  7.8 event on 20 July 2020, 99 km off the coast of  
Alaska), that may influence our calculation of PPSD. However, since we see no peak in the average ground motion at these  
245 times (e.g. no substantial peak in July 2020, Fig. 4), we suggest that teleseismic events are not majorly influencing our results.

One signal that does clearly influence our PPSD results in Fig. 4 is wind. Poor weather reported in the KSMMA, with wind  
gusts exceeding 80 km/hour at times were observed at the beginning of May, during an otherwise quiet period (i.e. no hydraulic  
fracturing operations in KSMMA, limited movement of people due to lockdown measures). Since the noise generated from  
250 wind gusts penetrates a wide frequency band, we are unable to filter it out. Using a filter between 4 and 14 Hz tries to eliminate  
some of these transient signals mostly associated with meteorological and oceanic conditions.

## 4.3 Generation of Latent Seismicity

The cessation of operations within the KSMMA in the summer of 2020 allows us a unique insight into seismicity that cannot  
be directly correlated with injection, which is the inferred triggering mechanism for most (if not all) of the seismicity within  
255 the KSMMA. The characteristics of the seismicity generated during this period suggest no fundamental differences in terms  
of temporal or spatial patterns or magnitudes to previous seismicity within the KSMMA that can be correlated with injection.



In fact, many of the characteristics appear to be equivalent to events detected prior to lockdown. Prior to the development of the Montney play, natural seismicity within the KSMMA was almost non-existent. The Canadian National Seismic Network (CNSN) recorded 20 earthquakes ( $M_L 2.5 - M_L 4.3$ ) from 1984 to 2008, which are assumed to be mostly natural events  
260 (Halchuk, 2009). The closest event to have occurred with a significantly larger magnitude than this occurred in March 1986 ( $M_w 5.4$ ) NE of Prince George, British Columbia (Lamontagne et al., 2008). In order to investigate the likelihood that our detected seismicity is natural seismicity, we calculate the expected recurrence rates of seismicity within the KSMMA greater than  $M_L 2.5$  from historical data, which is the magnitude of completeness used for the determination of seismic hazard maps in Canada due to detection thresholds from the Canadian public seismic network. The total number of earthquakes detected  
265 by the national network from 1984 to 2008 was 20 (Halchuk, 2009), suggesting a recurrence interval of 0.83 events per year. It is therefore unsurprising that during the period of quiescence, no events greater than  $M_L 2.5$  were detected. Following the Gutenberg-Richter formula (Gutenberg and Richter, 1944), it stands that there should be a 100-fold increase in the event rate to estimate the number of events  $>M_L 0.5$ , suggesting an event count of 83. Therefore, a maximum of 21% of events detected during relative quiescence can be attributed to natural seismicity. Therefore, over 70% of seismicity generated during  
270 this period of relative quiescence cannot be explained by this mechanism, and we suggest is likely produced as a remnant to previous operations, and therefore directly related to previous states of stress. With events being generated over 4 months since the cessation of operations, the state of stress at depth must be near-critical for an extended period of time in order to generate this “latent” seismicity.

275 The generation of seismicity in response to hydraulic fracturing is typically attributed to either fluid migration models, poroelastic phenomenon, or potentially aseismic slip (e.g. Bao and Eaton, 2016; Langenbruch and Zoback, 2016; Shapiro and Dinske, 2009; Segall and Lu, 2015; Eaton, 2018; Goebel and Brodsky, 2018; Eyre et al., 2019a). In the fluid migration model, pore fluid pressures are significantly increased upon fluid injection reducing the effective normal stress within a fault zone, which is sufficient to trigger seismicity (e.g. Peña Castro et al., 2020; Bao and Eaton, 2016). Given the temporal and spatial  
280 correlation between seismicity and hydraulic fracturing operations within the KSMMA, this appears to be a likely cause of seismicity. Under this model, the seismicity rate is usually observed to be proportional to the pore pressure, and is assumed to track the injection rate (Langenbruch and Zoback, 2016). Consequently, a slow and steady decrease in the rate of seismicity over time would be expected to occur, as fluid pressure leaks into the surrounding formations (Eyre et al., 2020), before seismicity returns to the background (i.e. natural) rate. Since seismicity during the period of quiescence is long-lived, shows no decay and  
285 cannot be attributed to increased fluid injection, another process must be involved in its generation. Furthermore, if pore fluid pressure and relaxation as a direct consequence of immediate injected fluid was the trigger of the seismicity during this period of quiescence, we would expect the seismicity to spatially migrate directly outwards from the most recently injected wells. We see no evidence of this (Fig. 5(b)), suggesting direct pore fluid migration cannot be held responsible for the triggering of this sequence.

290



Seismicity triggered by pore pressure diffusion can also be estimated by determining the propagating pore pressure fluid front ( $r_t$ ) related to the hydraulic diffusivity in a homogeneous isotropic saturated poroelastic medium (Shapiro and Dinske, 2009; Parotidis et al., 2003) by:

$$r_t = 4 * \pi * D * t, \quad (1)$$

295

where  $D$  is the hydraulic diffusivity and  $t$  is time since injection. If the triggering front ( $r_t$ ) closely follows the maximum distance of seismicity through time, then pore pressure diffusion is thought to play a central role in the triggering of this seismicity (e.g. Shapiro and Dinske, 2009; Parotidis et al., 2003). Diffusivity ( $D$ ) is generally assumed to range in the Earth's crust between  $0.1 \text{ m}^2/\text{s}$  and  $10 \text{ m}^2/\text{s}$  (Scholz, 2019), although in areas affected by hydraulic fracturing is thought to generally  
300 be in the range of  $0.1 \text{ m}^2/\text{s}$  to  $2 \text{ m}^2/\text{s}$  (e.g. Goebel et al., 2017; Shapiro and Dinske, 2009; Parotidis et al., 2003). Yu et al. (2019) suggested similar diffusivity values determined from seismicity related to hydraulic fracturing in the Montney formation to the NW of KSMMA, although others have speculated that much smaller diffusion values would be expected in shale formations (Eyre et al., 2020; Guglielmi et al., 2015). Higher values of diffusivity in hydraulic fracturing scenarios are anticipated due to faults and fractures at depth acting as fluid corridors (Caine et al., 1996), compared to in-tact shales. However, the seismicity  
305 generated in the KSMMA during the period of quiescence shows no coherence with a triggering front from the most recently active injection wells (Fig. 7), suggesting that pore pressure diffusion is not the dominant mechanism responsible for triggering these earthquakes.

Other models proposed for the generation of seismicity in response to hydraulic fracturing suggest that both pore pressure  
310 and poroelastic effects are feasible mechanisms (e.g. Segall and Lu, 2015; Goebel and Brodsky, 2018). In these instances, the increased pore pressure due to injection is thought to load the surrounding rock matrix, altering the stress field, often at great distances from the original injection site, if the region is well hydraulically connected. Again, however, this model suggests that seismicity is generated as a response to injecting fluid into the Earth, which was not occurring at the time of our latent seismicity. Given that the stress field would likely diminish following the cessation of fluid injection, we would also expect a  
315 decay in seismicity with time. We do not observe this. Alternatively, the trapping of fluids within a fault zone with only minor fluid migration along the fault, could result in slow changes to the effective stress due to changes in pore pressure (Sibson, 1992). In this method, seismicity should migrate spatially outwards from this fault zone as the effective stress migrates. We also see no evidence of this spatial migration (Fig. 5(b)).

320 Recently, Eyre et al. (2019a) have suggested that aseismic slip may play an important role in the generation of seismicity, whereby distal unstable regions of a fault are loaded by aseismic slip that initiated due to an increase in pore pressure within a stable zone, leading to the generation of seismicity. Once slip is initiated, far-field intraplate stresses may repeatedly reload unstable regions of the fault, leading to relatively steady seismicity rates. They suggest the driving stresses of such behaviour



are most likely to be elevated pore pressures (as a result of ongoing hydraulic fracturing in the area) becoming trapped within  
325 fault zones due to low permeabilities within many formations. Given that in the absence of the cessation of operations the  
detection of latent seismicity is extremely difficult, there are few examples of long-lived seismicity associated with hydraulic  
fracturing operations. One recent example comes from a long-lived seismic swarm in Alberta, where seismicity was observed  
over 10 months after injection ceased, and was interpreted as being driven primarily by aseismic slip (Eyre et al., 2020). We  
favour this interpretation of aseismic slip playing an important role in the initiation of seismicity since ongoing hydraulic  
330 fracturing operations are not required to generate ongoing seismicity; instead, the previous trapping of fluids within fault zones  
may be enough to sustain the generation of seismicity.

It is widely reported that earthquakes can be generated by transient stress changes related to the passage of seismic waves  
(i.e. “dynamic triggering”, (e.g. Wang et al., 2015; Van der Elst et al., 2013; Hill and Prejean, 2007)). In some cases, this  
335 dynamic triggering can also be delayed by days or weeks following a teleseism, potentially related to the re-distribution of  
pore fluid from the passing seismic waves (Brodsky and Prejean, 2005) or through initial aseismic slip on faults triggering  
seismicity (Shelly et al., 2011). During the period of quiescence (28 March to 6 August 2020), 43 earthquakes of  $>M6$  were  
reported by the United States Geological Survey (2020), that may have the potential to cause dynamic triggering. We follow the  
methodology set out by Wang et al. (2015), whereby we first select only the teleseismic events that generated an estimated peak  
340 ground velocity of greater than 0.2 cm/s at any station within the KSMMA, as defined by Lay and Wallace (1995), whereby:

$$\log A_{20} = M - 1.66 \log_{10} \delta - 2, \quad (2)$$

and:

$$PGV \approx \frac{2\pi A_{20}}{T} \quad (3)$$

where  $A_{20}$  is the peak waveform amplitude when filtered at 20s;  $M$  is the magnitude;  $\delta$  is the epicenter-station distance (in  
345 degrees); and  $T$  is the surface wave period (assumed to be 20 s). This method identified 40 events from the original list of  
teleseismic events. We then calculated the  $\beta$  statistic (Matthews and Reasenberg, 1988) by:

$$\beta(N_1, N_2, t_1, t_2) = \frac{N_2 - E(N_2)}{\sqrt{\text{var}(N_2)}}, \quad (4)$$

which is a quantitative measure of the level of dynamic triggering, representing the standard deviation in the background  
seismicity rate after a remote event.  $N_1$  and  $N_2$  are the number of earthquakes detected before ( $t_1$ ) and after ( $t_2$ ) the remote  
350 event, respectively. Here, we take  $t_1$  and  $t_2$  to be 12 hours.  $E(N_2) = N_1 t_2 / t_1$  is the expected number of earthquakes after  
the main shock based on the background seismicity rate. If no earthquakes occur in  $t_1$  (i.e. before the main shock),  $N_1$  is set  
to 0.25 based on the equivalent range of the probability density function (Matthews and Reasenberg, 1988; Hill and Prejean,



2007). When  $\beta \geq 2$ , there is sufficient statistical evidence (at a 95% confidence level) that there is a significant increase in the seismic event rate following the remote event (Hill and Prejean, 2007).

355

We identify 7 remote earthquakes that generate a  $\beta$  value  $\geq 2$  (Fig. 8), including the largest magnitude event to have occurred to date in 2020 that occurred 99 km SSE of Perryville, Alaska on 22 July at 06:12 UTC, with  $M_w$  7.8 (United States Geological Survey, 2020), although the increase in event count in the KSMMA following this remote event is difficult to determine without statistical analysis. In some cases however, such as following the  $M_w$  6.1 event on 31 May 2020, 43 km W of Lampa, Peru, a significant increase in the number of events detected in KSMMA is clear. Our analysis therefore suggests that a maximum of 8% of the seismicity detected during this period of relative quiescence may be attributed to dynamic triggering, in particular the events on 31 May 2020, however  $<70\%$  of the detected seismicity cannot be attributed to primary activation mechanisms such as this, and therefore in our opinion are the result of “latent” ongoing processes.

360

## 5 Conclusions

Seismicity generated in the KSMMA has always been attributed to oil and gas recovery in the area, primarily due to its temporal and spatial correlation to operations. However, during the COVID-19 pandemic in the summer of 2020, operations in the KSMMA were halted. Despite this, 389 seismic events were recorded by our seismic network. These events occurred within the spatial extent of previous events in the area (a corridor orientated NW-SE), and had similar magnitudes to previously recorded seismicity ( $\sim M_L - 1$  to  $M_L 1.2$ ). The low magnitude of completeness ( $M_c = 0.4$ ) is indicative of the general quietening of the area, as operations and the movement of people were restricted with government regulations. The  $b$ -value of generated seismicity ( $\sim 1.96$ ) is similar to previous estimates within areas dominated by hydraulic fracturing. Unlike during active hydraulic fracturing operations, events showed no temporal clustering, but instead were generated in a fairly constant manner over the  $\sim 4$  months of quiescence. No spatial correlation between the most recently active wells in the area and seismicity could be determined, however the fact that seismicity occurs at the depths of previous injection (i.e. the target formations) suggests that the area must be hydraulically linked.

370

375

Since there is no temporal or spatial evidence that these events are a direct consequence of the most recent hydraulic fracturing in the area (i.e. an aftershock sequence driven by pore pressure diffusion or poroelastic relaxation), and since the area is typically naturally quiet seismically (a maximum of 21% of the detected events), we conclude that most of these events are an indirect response of the increased pore pressures at depth which is causing aseismic slip on already pressurized fault zones, as a result of previous fluid injection in the area. A number of events may be the result of dynamic triggering, from remote events with  $M_w > 6$  (up to  $\sim 8\%$ ), however this process cannot account for the majority of the seismicity observed ( $>70\%$ ). We suggest that the prior fluid injection in the area has altered the state of stress, and caused fluids to become trapped in fault and fracture zones at depth. This allows seismicity to be primarily generated by aseismic slip loading unstable regions of these

380



385 pressurized zones at depth. Once slip has initiated, far-field stresses may repeatedly reload these unstable zones, leading to the relatively stable seismicity rate that is observed.

*Code and data availability.* Continuous seismic data, station and associated metadata for the EO network is available through Incorporated Research Institutions for Seismology (IRIS) (<http://ds.iris.edu/ds/nodes/dmc/>) using Network Code EO, following a 91-day embargo period. The velocity model used for location analysis is available directly from the British Columbia Oil and Gas Commission. Seismic noise analysis  
390 (e.g. Figs 1 and 4) were envisaged by Thomas Lecocq; the code can be found here: <https://github.com/ThomasLecocq/SeismoRMS>.

*Author contributions.* ROS contributed to the conceptualization, analyzed the data, wrote the manuscript and was primarily responsible for this research, with guidance, comments and revisions from DWE.

*Competing interests.* The authors declare that they have no conflict of interest.

*Acknowledgements.* The authors thank Geoscience BC for funding this project. We also acknowledge our industry partners whose collaboration  
395 enabled the installation of this network, including ARC resources, Canadian Natural Resources Ltd., and the Natural Sciences and Engineering Research Council of Canada for providing further funding for this project. Further support was provided through the Microseismic Industry Consortium. Nanometrics is gratefully acknowledged for their contribution to this project, including the installation and maintenance of stations, and near real-time analysis of seismicity including the generation of the catalogue of seismic events. We would like to thank those at the Incorporated Research Institutions for Seismology (IRIS) for hosting the data and facilitating collaboration. We would especially like  
400 to thank Jay Hogan at Nanometrics who facilitated the successful upload of data to IRIS. We would like to thank Thomas H. A. Swinscoe (University of Calgary) for producing Fig. 2, which was produced using QGIS (<https://qgis.org/en/site/about/index.html>) and Thomas Lecocq (Royal Observatory Belgium) for codes that led to the development of Figs. 1 and 4. Figure 5(b) was produced using GMT v.6 (Wessel et al., 2019). Seismic analysis was carried out using the Obspy Python package (Beyreuther et al., 2010).



## References

- 405 Amini, A. and Eberhardt, E.: Influence of tectonic stress regime on the magnitude distribution of induced seismicity events related to hydraulic fracturing, *Journal of Petroleum Science and Engineering*, 182, 106284, <https://doi.org/10.1016/j.petrol.2019.106284>, 2019.
- Anthony, R. E., Ringler, A. T., Wilson, D. C., Bahavar, M., and Koper, K. D.: How processing methodologies can distort and bias power spectral density estimates of seismic background noise, *Seismological Research Letters*, 91, 1694–1706, <https://doi.org/10.1785/0220190212>, 2020.
- 410 Armitage, J.: Triassic oil and gas occurrences in northeastern British Columbia, Canada, *Bulletin of Canadian Petroleum Geology*, 10, 35–56, <http://archives.datapages.com/data/cspg/data/010/010002/0035.htm>, 1962.
- Atkinson, G. M., Eaton, D. W., Ghofrani, H., Walker, D., Cheadle, B., Schultz, R., Shcherbakov, R., Tiampo, K., Gu, J., Harrington, R. M., et al.: Hydraulic fracturing and seismicity in the Western Canada Sedimentary Basin, *Seismological Research Letters*, 87, 631–647, <https://doi.org/10.1785/0220150263>, 2016.
- 415 Babaie-Mahani, A. and Kao, H.: Determination of Local Magnitude for Induced Earthquakes in the Western Canada Sedimentary Basin: An Update, *CSEG Recorder*, 45, <https://csegrecorder.com/articles/view/determination-of-local-magnitude-for-induced-earthquakes-in-the-wcsb>, 2020.
- Babaie-Mahani, A., Kao, H., Atkinson, G. M., Assatourians, K., Addo, K., and Liu, Y.: Ground-motion characteristics of the 30 November 2018 injection-induced earthquake sequence in Northeast British Columbia, Canada, *Seismological Research Letters*, 90, 1457–1467, 420 <https://doi.org/10.1785/0220190040>, 2019.
- Bao, X. and Eaton, D. W.: Fault activation by hydraulic fracturing in western Canada, *Science*, 354, 1406–1409, <https://doi.org/10.1126/science.aag2583>, 2016.
- Barclay, J., Krause, F., Campbell, R., and Utting, J.: Dynamic casting and growth faulting: Dawson Creek graben complex, Carboniferous–Permian Peace River embayment, western Canada, *Bulletin of Canadian Petroleum Geology*, 38, 115–145, 425 <https://doi.org/10.35767/gscpgbull.38a.1.115>, 1990.
- BC Oil and Gas Commission: Order 18-90-001 (Amendment Number 1) – Kiskatinaw Seismic Monitoring and Mitigation Area Special Project Order, Online, <https://www.bcogc.ca/files/reports/Technical-Reports/Kiskatinaw-Seismic-Monitoring-and-Mitigation-Area-KSMMA-Special-Project-Order-18-90-001-Amendment-1.pdf>, 2018.
- Beyreuther, M., Barsch, R., Krischer, L., Megies, T., Behr, Y., and Wassermann, J.: ObsPy: A Python toolbox for seismology, *Seismological Research Letters*, 81, 530–533, <https://doi.org/10.1785/gssrl.81.3.530>, 2010. 430
- Brodsky, E. E. and Prejean, S. G.: New constraints on mechanisms of remotely triggered seismicity at Long Valley Caldera, *Journal of Geophysical Research: Solid Earth*, 110, <https://doi.org/10.1029/2004JB003211>, 2005.
- Buurman, H. and West, M. E.: Seismic Precursors to Volcanic Explosions During the 2006 Eruption of Augustine Volcano, in: *The 2006 Eruption of Augustine Volcano, Alaska*, edited by Power, J. A., Coombs, M. L., and Freymueller, J., U.S. Geological Survey Professional Paper 1769, [https://pubs.usgs.gov/pp/1769/chapters/p1769\\_chapter02.pdf](https://pubs.usgs.gov/pp/1769/chapters/p1769_chapter02.pdf), 2010. 435
- Caine, J. S., Evans, J. P., and Forster, C. B.: Fault zone architecture and permeability structure, *Geology*, 24, 1025–1028, [https://doi.org/10.1130/0091-7613\(1996\)024<1025:FZAAPS>2.3.CO;2](https://doi.org/10.1130/0091-7613(1996)024<1025:FZAAPS>2.3.CO;2), 1996.
- Chouet, B. A.: Long-period volcano seismicity: its source and use in eruption forecasting, *Nature*, 380, 309–316, <https://doi.org/10.1038/380309a0>, 1996.



- 440 Dias, F. L., Assumpção, M., Peixoto, P. S., Bianchi, M. B., Collaço, B., and Calhau, J.: Using Seismic Noise Levels to Monitor Social Isolation: An Example from Rio de Janeiro, Brazil, *Geophysical Research Letters*, 47, e2020GL088748, <https://doi.org/10.1029/2020GL088748>, 2020.
- Dixon, J.: Regional lithostratigraphic units in the Triassic Montney Formation of western Canada, *Bulletin of Canadian Petroleum Geology*, 48, 80–83, <https://doi.org/10.2113/48.1.80>, 2000.
- 445 Eaton, D. W.: *Passive seismic monitoring of induced seismicity: Fundamental principles and application to energy technologies*, Cambridge University Press, 2018.
- Eaton, D. W. and Maghsoudi, S.: 2b... or not 2b? Interpreting magnitude distributions from microseismic catalogs, *First Break*, 33, <https://doi.org/10.3997/1365-2397.33.10.83159>, 2015.
- Eaton, D. W. and Schultz, R.: Increased likelihood of induced seismicity in highly overpressured shale formations, *Geophysical Journal International*, 214, 751–757, <https://doi.org/10.1093/gji/ggy167>, 2018.
- 450 Eaton, D. W., Davidsen, J., Pedersen, P. K., and Boroumand, N.: Breakdown of the Gutenberg-Richter relation for microearthquakes induced by hydraulic fracturing: influence of stratabound fractures, *Geophysical Prospecting*, 62, 806–818, <https://doi.org/10.1111/1365-2478.12128>, 2014.
- Ellsworth, W. L.: Injection-induced earthquakes, *Science*, 341, <https://doi.org/10.1126/science.1225942>, 2013.
- 455 Eyre, T. S., Eaton, D. W., Garagash, D. I., Zecevic, M., Venieri, M., Weir, R., and Lawton, D. C.: The role of aseismic slip in hydraulic fracturing-induced seismicity, *Science Advances*, 5, eaav7172, <https://doi.org/10.1126/sciadv.aav7172>, 2019a.
- Eyre, T. S., Eaton, D. W., Zecevic, M., D'Amico, D., and Kolos, D.: Microseismicity reveals fault activation before Mw 4.1 hydraulic-fracturing induced earthquake, *Geophysical Journal International*, 218, 534–546, <https://doi.org/10.1093/gji/ggz168>, 2019b.
- Eyre, T. S., Zecevic, M., Salvage, R. O., and Eaton, D. W.: A long-lived swarm of hydraulic fracturing-induced seismicity provides evidence for aseismic slip, *Bulletin of the Seismological Society of America*, 110, 2205–2215, <https://doi.org/10.1785/0120200107>, 2020.
- 460 Furlong, C. M., Gingras, M. K., and Zonneveld, J.-P.: High-resolution sequence stratigraphy of the Middle Triassic Sunset Prairie Formation, Western Canada Sedimentary Basin, north-eastern British Columbia, *The Depositional Record*, 6, 383–408, <https://doi.org/10.1002/dep2.107>, 2020.
- Goebel, T., Weingarten, M., Chen, X., Haffener, J., and Brodsky, E.: The 2016 Mw 5.1 Fairview, Oklahoma earthquakes: Evidence for long-range poroelastic triggering at > 40 km from fluid disposal wells, *Earth and Planetary Science Letters*, 472, 50–61, <https://doi.org/10.1016/j.epsl.2017.05.011>, 2017.
- 465 Goebel, T. H. and Brodsky, E. E.: The spatial footprint of injection wells in a global compilation of induced earthquake sequences, *Science*, 361, 899–904, <https://doi.org/10.1126/science.aat5449>, 2018.
- Guglielmi, Y., Elsworth, D., Cappa, F., Henry, P., Gout, C., Dick, P., and Durand, J.: In situ observations on the coupling between hydraulic diffusivity and displacements during fault reactivation in shales, *Journal of Geophysical Research: Solid Earth*, 120, 7729–7748, <https://doi.org/10.1002/2015JB012158>, 2015.
- 470 Gutenberg, B. and Richter, C. F.: Frequency of earthquakes in California, *Bulletin of the Seismological Society of America*, 34, 185–188, <https://core.ac.uk/download/pdf/33111762.pdf>, 1944.
- Halchuk, S.: *Seismic Hazard Earthquake Epicentre File (SHEEF) used in the fourth generation seismic hazard maps of Canada*, Tech. rep., Geological Survey of Canada, Open File 6208, <https://doi.org/10.4095/261333>, 2009.
- 475 Hill, D. and Prejean, S.: 4.09 - Dynamic Triggering, in: *Treatise on Geophysics*, edited by Schubert, G., pp. 257 – 291, Elsevier, Amsterdam, 2007.



- Hutton, L. and Boore, D. M.: The ML scale in southern California, *Bulletin of the Seismological Society of America*, 77, 2074–2094, [https://pubs.geoscienceworld.org/ssa/bssa/article/77/6/2074/119025?casa\\_token=HlkEaVCYcsgAAAAA:FH2P5kTt4O-RJs4yC1b52wEA\\_OhyoVcfBUhyszqplA5TZTSobbAD5WXraQTV1jiv1DnkWQ0](https://pubs.geoscienceworld.org/ssa/bssa/article/77/6/2074/119025?casa_token=HlkEaVCYcsgAAAAA:FH2P5kTt4O-RJs4yC1b52wEA_OhyoVcfBUhyszqplA5TZTSobbAD5WXraQTV1jiv1DnkWQ0), 1987.
- 480 OhyoVcfBUhyszqplA5TZTSobbAD5WXraQTV1jiv1DnkWQ0, 1987.
- Igonin, N., Zecevic, M., and Eaton, D. W.: Bilinear magnitude–frequency distributions and characteristic earthquakes during hydraulic fracturing, *Geophysical Research Letters*, 45, 12–866, <https://doi.org/10.1029/2018GL079746>, 2018.
- Lahr, J. C., Chouet, B. A., Stephens, C. D., Power, J. A., and Page, R. A.: Earthquake classification, location, and error analysis in a volcanic environment: Implications for the magmatic system of the 1989–1990 eruptions at Redoubt Volcano, Alaska, *Journal of Volcanology and*
- 485 *Geothermal Research*, 62, 137–151, [https://doi.org/10.1016/0377-0273\(94\)90031-0](https://doi.org/10.1016/0377-0273(94)90031-0), 1994.
- Lamontagne, M., Halchuk, S., Cassidy, J., and Rogers, G.: Significant Canadian earthquakes of the period 1600–2006, *Seismological Research Letters*, 79, 211–223, <https://doi.org/10.1785/gssrl.79.2.211>, 2008.
- Langenbruch, C. and Zoback, M. D.: How will induced seismicity in Oklahoma respond to decreased saltwater injection rates?, *Science Advances*, 2, e1601542, <https://doi.org/10.1126/sciadv.1601542>, 2016.
- 490 Lay, T. and Wallace, T. C.: *Modern global seismology*, Elsevier, 1995.
- Lecocq, T., Hicks, S. P., Van Noten, K., van Wijk, K., Koelemeijer, P., De Plaen, R. S., Massin, F., Hillers, G., Anthony, R. E., Apoloner, M.-T., et al.: Global quieting of high-frequency seismic noise due to COVID-19 pandemic lockdown measures, *Science*, 369, 1338–1343, <https://doi.org/10.1126/science.abd2438>, 2020.
- Lomax, A., Virieux, J., Volant, P., and Berge-Thierry, C.: Probabilistic earthquake location in 3D and layered models, in: *Advances in seismic event location*, pp. 101–134, Springer, [https://doi.org/10.1007/978-94-015-9536-0\\_5](https://doi.org/10.1007/978-94-015-9536-0_5), 2000.
- 495 Lomax, A., Michelini, A., and Curtis, A.: Earthquake location, direct, global-search methods, *Encyclopedia of complexity and systems science*, 5, 2449–2473, <https://core.ac.uk/download/pdf/41147529.pdf>, 2009.
- Matthews, M. V. and Reasenber, P. A.: Statistical methods for investigating quiescence and other temporal seismicity patterns, *Pure and Applied Geophysics*, 126, 357–372, <https://doi.org/10.1007/BF00879003>, 1988.
- 500 McNamara, D. E. and Buland, R. P.: Ambient noise levels in the continental United States, *Bulletin of the Seismological Society of America*, 94, 1517–1527, <https://doi.org/10.1785/012003001>, 2004.
- Nieto, J., Bialowas, B., Batlai, B., and Janega, G.: Managing Induced Seismicity in Cambrian’s Altares Field in the Montney Formation, N.E. British Columbia - An Update, *CSEG Recorder*, 43, <https://csegrecorder.com/articles/view/managing-induced-seismicity-in-cambriams-altares-field-in-the-montney-fm>, 2018.
- 505 Parotidis, M., Rothert, E., and Shapiro, S.: Pore-pressure diffusion: A possible triggering mechanism for the earthquake swarms 2000 in Vogtland/NW-Bohemia, central Europe, *Geophysical Research Letters*, 30, <https://doi.org/10.1029/2003GL018110>, 2003.
- Peña Castro, A., Roth, M., Verdecchia, A., Onwuemeka, J., Liu, Y., Harrington, R., Zhang, Y., and Kao, H.: Stress Chatter via Fluid Flow and Fault Slip in a Hydraulic Fracturing-Induced Earthquake Sequence in the Montney Formation, British Columbia, *Geophysical Research Letters*, 47, e2020GL087254, <https://doi.org/10.1029/2020GL087254>, 2020.
- 510 Richter, C. F.: An instrumental earthquake magnitude scale, *Bulletin of the Seismological Society of America*, 25, 1–32, [https://pubs.geoscienceworld.org/ssa/bssa/article/25/1/1/115102?casa\\_token=TJcAnX3xa50AAAAA:pAhONJN1dQBXeY95QN\\_bnfvBrBaIGmwg6KQqgSni8n5uARZ-3qAimCFTWzzFjncCglSzyag](https://pubs.geoscienceworld.org/ssa/bssa/article/25/1/1/115102?casa_token=TJcAnX3xa50AAAAA:pAhONJN1dQBXeY95QN_bnfvBrBaIGmwg6KQqgSni8n5uARZ-3qAimCFTWzzFjncCglSzyag), 1935.
- Salvage, R. O., Dettmer, J., Swinscoe, T. H. A., MacDougall, K., Eaton, D. W., Stacey, M., Aboud, M., Kang, T.-S., Kim, S., and J., R.: Real-Time Monitoring of Seismic Activity in the Kiskatinaw Area, Northeastern British Columbia (NTS 093P, 094A), Tech. rep., *Geoscience BC Summary of Activities 2020: Energy and Water*, Geoscience BC, Report 2021-2, 2021.
- 515



- Scholz, C. H.: The mechanics of earthquakes and faulting, Cambridge university press, 2019.
- Schorlemmer, D., Wiemer, S., and Wyss, M.: Variations in earthquake–size distribution across different stress regimes, *Nature*, 437, 539–542, <https://doi.org/10.1038/nature04094>, 2005.
- Schultz, R., Stern, V., and Gu, Y. J.: An investigation of seismicity clustered near the Cordell Field, west central Alberta, and its relation to a nearby disposal well, *Journal of Geophysical Research: Solid Earth*, 119, 3410–3423, <https://doi.org/10.1002/2013JB010836>, 2014.
- Segall, P. and Lu, S.: Injection–induced seismicity: Poroelastic and earthquake nucleation effects, *Journal of Geophysical Research: Solid Earth*, 120, 5082–5103, <https://doi.org/10.1002/2015JB012060>, 2015.
- Shapiro, S. A. and Dinske, C.: Fluid–induced seismicity: Pressure diffusion and hydraulic fracturing, *Geophysical Prospecting*, 57, 301–310, <https://doi.org/10.1111/j.1365-2478.2008.00770.x>, 2009.
- 525 Shelly, D. R., Peng, Z., Hill, D. P., and Aiken, C.: Triggered creep as a possible mechanism for delayed dynamic triggering of tremor and earthquakes, *Nature Geoscience*, 4, 384–388, <https://doi.org/10.1038/ngeo1141>, 2011.
- Sibson, R. H.: Implications of fault–valve behaviour for rupture nucleation and recurrence, *Tectonophysics*, 211, 283–293, [https://doi.org/10.1016/0040-1951\(92\)90065-E](https://doi.org/10.1016/0040-1951(92)90065-E), 1992.
- Skoumal, R. J., Brudzinski, M. R., and Currie, B. S.: Distinguishing induced seismicity from natural seismicity in Ohio: Demonstrating the utility of waveform template matching, *Journal of Geophysical Research: Solid Earth*, 120, 6284–6296, <https://doi.org/10.1002/2015JB012265>, 2015.
- 530 United States Geological Survey: Earthquake Catalog, Online, <https://earthquake.usgs.gov/earthquakes/search/>, last Accessed: November 2020, 2020.
- Van der Elst, N. J., Savage, H. M., Keranen, K. M., and Abers, G. A.: Enhanced remote earthquake triggering at fluid-injection sites in the midwestern United States, *Science*, 341, 164–167, <https://doi.org/10.1126/science.1238948>, 2013.
- 535 Visser, R., Kao, H., Smith, B., Goerzen, C., Kontou, B., Dokht, R. M. H., Hutchinson, J., Tan, F., and Babaie-Mahani, A.: A comprehensive earthquake catalogue for the Fort St. John–Dawson Creek region, British Columbia, 2017–2018, Tech. rep., Geological Survey of Canada, Open File 8718, <https://doi.org/10.4095/326015>, 2020.
- Waldhauser, F. and Ellsworth, W. L.: A double-difference earthquake location algorithm: Method and application to the northern Hayward fault, California, *Bulletin of the Seismological Society of America*, 90, 1353–1368, <https://doi.org/10.1785/0120000006>, 2000.
- 540 Wang, B., Harrington, R. M., Liu, Y., Yu, H., Carey, A., and van der Elst, N. J.: Isolated cases of remote dynamic triggering in Canada detected using cataloged earthquakes combined with a matched–filter approach, *Geophysical Research Letters*, 42, 5187–5196, <https://doi.org/10.1002/2015GL064377>, 2015.
- Welch, P.: The use of fast Fourier transform for the estimation of power spectra: a method based on time averaging over short, modified periodograms, *IEEE Transactions on audio and electroacoustics*, 15, 70–73, <https://doi.org/10.1109/TAU.1967.1161901>, 1967.
- 545 Wessel, P., Luis, J., Uieda, L., Scharroo, R., Wobbe, F., Smith, W., and Tian, D.: The Generic Mapping Tools version 6, *Geochemistry, Geophysics, Geosystems*, 20, 5556–5564, <https://doi.org/10.1029/2019GC008515>, 2019.
- Wessels, S. A., De La Peña, A., Kratz, M., Williams-Stroud, S., and Jbeili, T.: Identifying faults and fractures in unconventional reservoirs through microseismic monitoring, *First break*, 29, <https://doi.org/10.3997/1365-2397.29.7.51919>, 2011.
- 550 Yu, H., Harrington, R., Liu, Y., and Wang, B.: Induced seismicity driven by fluid diffusion revealed by a near-field hydraulic stimulation monitoring array in the Montney Basin, British Columbia, *Journal of Geophysical Research: Solid Earth*, 124, 4694–4709, <https://doi.org/10.1029/2018JB017039>, 2019.

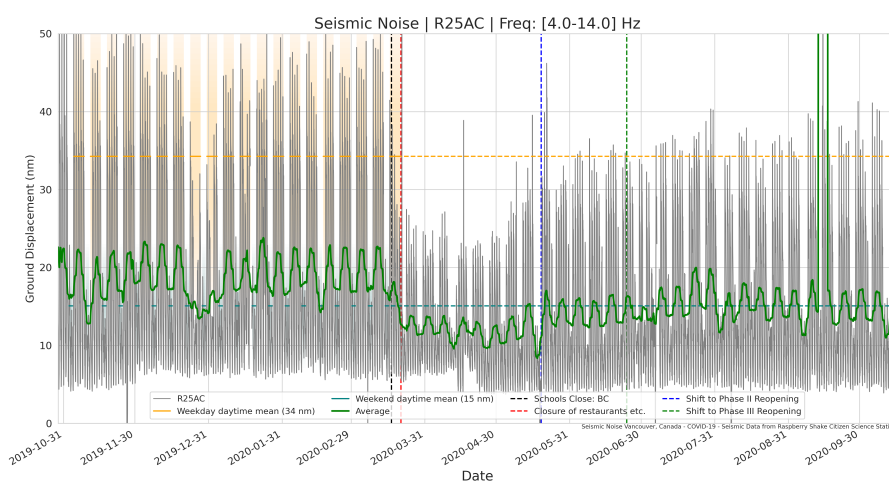


**Figure 1.** Filtered (4-14Hz) ambient seismic noise displayed as displacement from station R25AC (Z component) located in Vancouver, British Columbia. 30-minute average PPSD (dark grey), with rolling mean (window size = 92 hours) shown in green. The timing of different lockdown scenarios for British Columbia are shown as vertical dashed lines. A clear reduction in the ground motion is observed following initial lockdown conditions in March 2020. The large peak in noise in September is thought to be meteorological, rather than a sudden increase in anthropogenic activity. Figure courtesy of codes developed by Thomas Lecocq and Fred Massin.

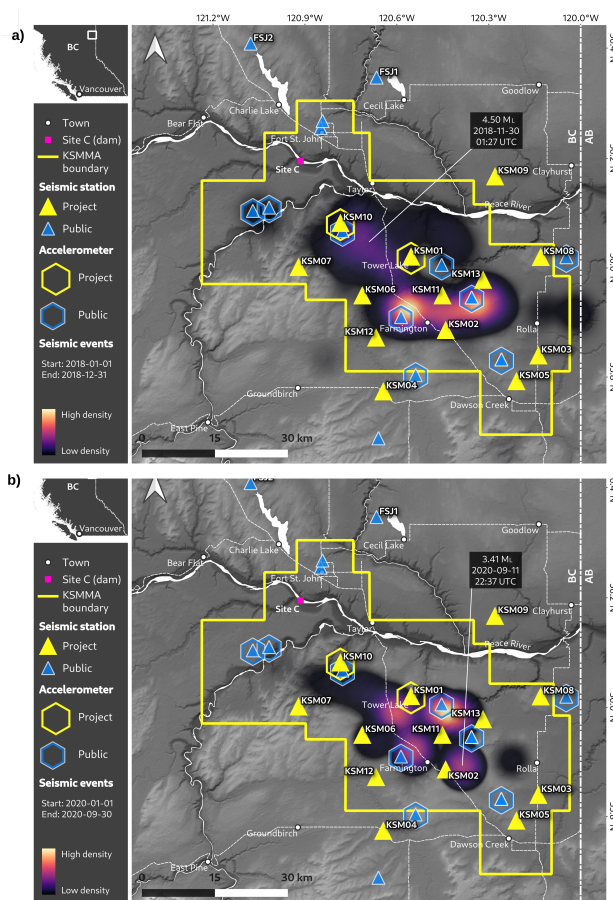


**Figure 2.** Spatial locations of seismicity concentrations within the KSMMA. Higher density of seismic events is indicated by brighter colours; lower density by darker colours; and no seismicity by grey. The outline of the KSMMA boundary is shown in yellow; public seismic monitoring stations as blue triangles; the newly installed EO network as yellow triangles; and co-located accelerometers as hexagons. FSJ1 and FSJ2 are also part of the EO network but were installed in 2018. FSJ1 was decommissioned on 26 August 2020 but is shown for completeness as it was used in seismic analysis prior to this. The largest measured magnitude event within the KSMMA boundary is marked. (a) Seismic events reported by NRCan between 1 January 2018 and 31 December 2018 (Visser et al., 2020). Note: although the new dense array was not installed at this time, it is shown on the map for reference. The largest event in 2018, occurring on 30 November, north of Tower Lake is shown ( $M_L$  4.5). (b) Seismic events recorded on the newly installed EO network (and incorporating data from public stations) from 22 January 2020 to 30 September 2020. The largest magnitude event, occurring on 11 September 2020 is indicated ( $M_L$  3.4). Figure courtesy of Thomas H. A. Swincoe, using QGIS (<https://qgis.org/en/site/about/index.html>).

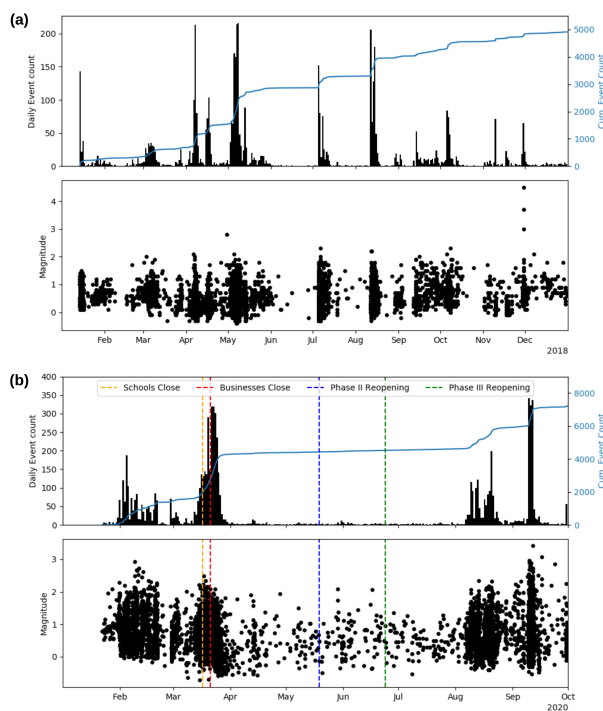


**Figure 3.** Temporal evolution of seismicity within the KSMMA (daily counts in black, cumulative counts in blue). Magnitudes calculated using the  $M_L$  formula of Hutton and Boore (1987). Distinct temporal patterns can be observed in both years, associated with ongoing hydraulic fracturing operations in the area. *Note: the different time (x-axis) scales.* (a) Seismicity within the KSMMA in 2018 from catalogue of Visser et al. (2020). (b) Seismicity within the KSMMA in 2020 from catalogue derived by the newly installed network (yellow triangles, Fig. 2). The timing of different lockdown scenarios affecting the KSMMA are shown as vertical dashed lines. The time period from April to August 2020 represents the period of relative quiescence due to the COVID-19 lockdown. The time lag for seismicity build up after the Phase III reopening reflects the time required for operations in the area to be restarted.

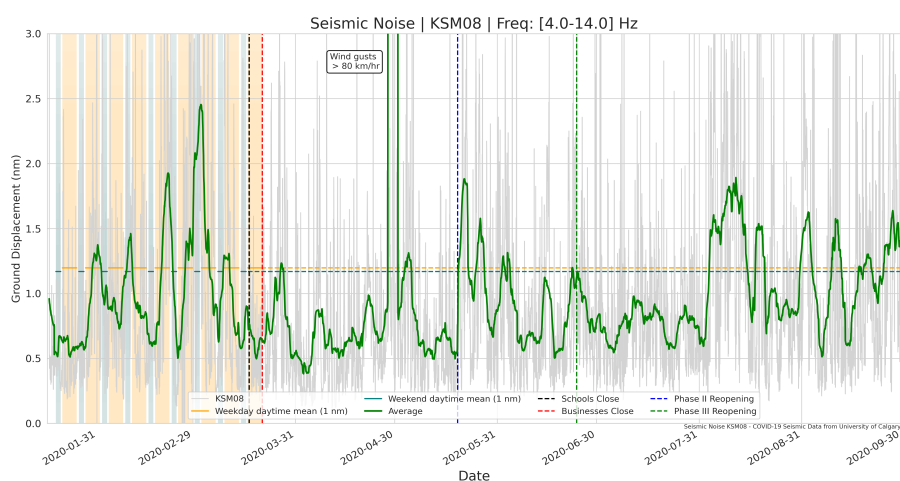


**Figure 4.** Filtered (4-14Hz) ambient seismic noise displayed as displacement from station KSM08 (Z component) located within the KSMMA. 30-minute average PPSD (dark grey), with rolling mean (window size = 92 hours) shown in green. The timing of different lockdown scenarios for British Columbia are shown as vertical dashed lines. A clear reduction in the ground motion is observed following initial lockdown conditions in March 2020, and significant increases in ground motion as lockdown measures are rescinded. Figure courtesy of codes developed by Thomas Lecocq and Fred Massin.

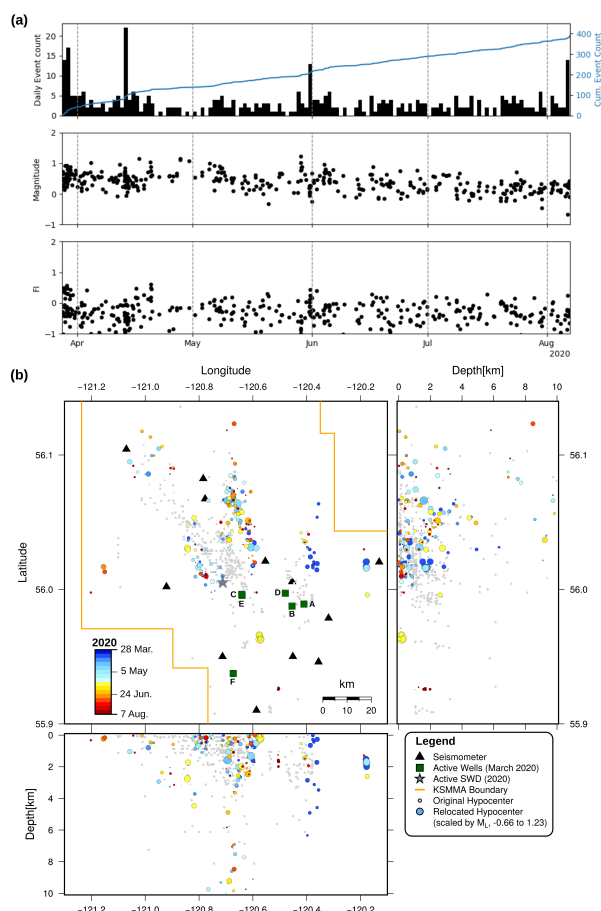


**Figure 5.** Temporal and spatial evolution of 389 events detected in the KSMMA during the cessation of operations from April to August 2020. (a) *Upper:* Daily event count and cumulative event counts. *Middle:*  $M_L$  determined using the formula of Babaie-Mahani and Kao (2020). *Lower:* Frequency Index (FI) detailing the ratio of high frequency energy to low frequency energy within each detected waveform at KSM06. (b) Spatial evolution of events coloured by time and scaled by magnitude. Active wells that initiated seismicity in the month prior to quiescence (March 2020) are shown as green squares labelled A (most recently active prior to lockdown i.e. late March 2020) to E (active in early March); one active SWD well is shown as the grey star. Figure generated using GMT v.6 (Wessel et al., 2019).

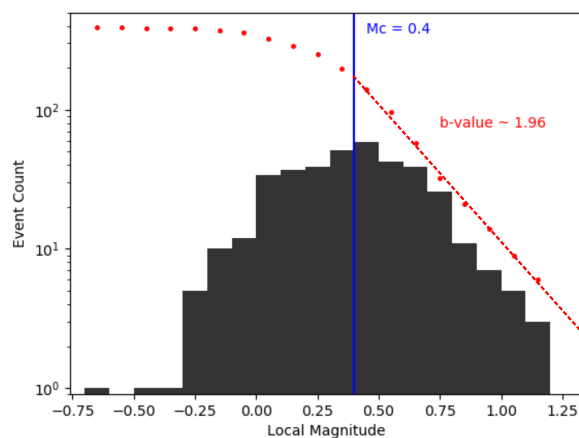


**Figure 6.** Frequency-Magnitude distribution of events ( $n=389$ ) detected in the KSMMA during quiescence from 28 March to 6 August 2020. Event counts in magnitude bins of 0.1 are shown as black columns; the cumulative event value per bin is shown as a red dot. The magnitude of completeness ( $M_c$ ) is 0.4, and the estimated  $b$ -value is 1.96 (Gutenberg and Richter, 1944).

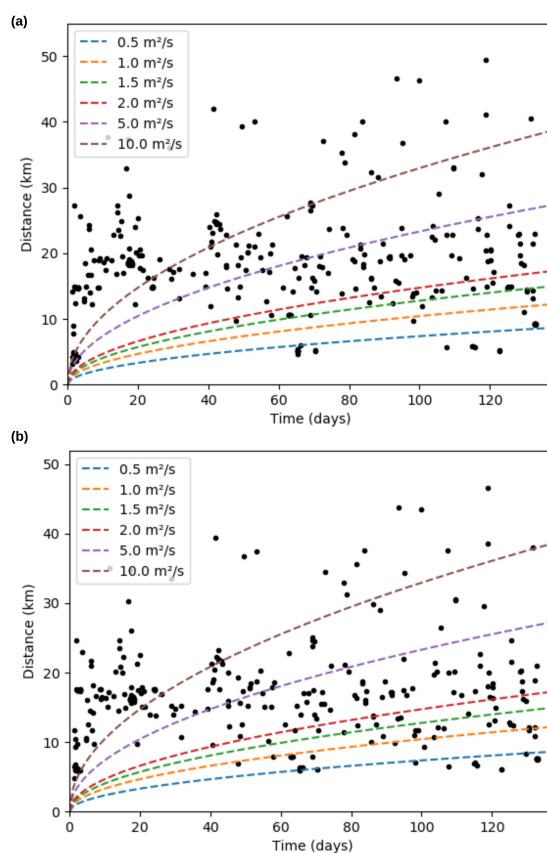


**Figure 7.** Time-distance plots of latent seismicity from 28 March to 6 August 2020. (a) Distance of events measured away from Well A (Fig. 5) and time zero taken as the last day of injection at this well prior to lockdown (27 March 2020). (b) Distance of events measured away from Well B (Fig. 5) and time zero taken as the last day of injection at this well prior to lockdown (27 March 2020). Representative diffusion curves associated with hydraulic fracturing and waste-water injection (Goebel et al., 2017; Shapiro and Dinske, 2009) are shown. The events during quiescence in the KSMMA cannot be successfully modelled using pore pressure diffusion suggesting it cannot be a primary mechanism for generating this seismicity.

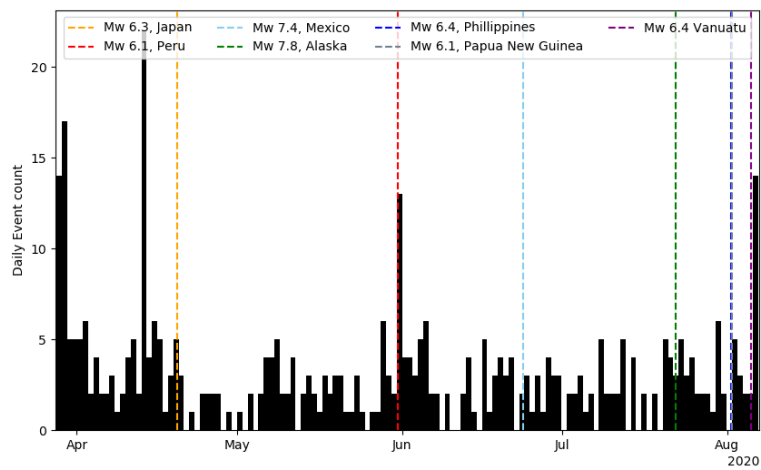


**Figure 8.** Teleseismic events (dotted vertical lines) that statistically (95% confidence level) generated dynamic triggering of seismicity within the KSMMA.